Anomalous Scaling of Aeolian Sand Transport Reveals Coupling to Bed Rheology

Katharina Tholen,[1] Thomas Pähtz,[2,3,*] Sandesh Kamath,[4] Eric J. R. Parteli,[4] and Klaus Kroy[1,†]
[1]*Institute for Theoretical Physics, Leipzig University, Postfach 100920, 04009 Leipzig, Germany*
[2]*Donghai Laboratory, 316021 Zhoushan, China*
[3]*Institute of Port, Coastal and Offshore Engineering, Ocean College, Zhejiang University, 316021 Zhoushan, China*
[4]*Faculty of Physics, University of Duisburg-Essen, Lotharstraße 1-21, D-47057 Duisburg, Germany*

(Received 5 August 2022; accepted 5 January 2023; published 3 February 2023)

Predicting transport rates of windblown sand is a central problem in aeolian research, with implications for climate, environmental, and planetary sciences. Though studied since the 1930s, the underlying many-body dynamics is still incompletely understood, as underscored by the recent empirical discovery of an unexpected third-root scaling in the particle-fluid density ratio. Here, by means of grain-scale simulations and analytical modeling, we elucidate how a complex coupling between grain-bed collisions and granular creep within the sand bed yields a dilatancy-enhanced bed erodibility. Our minimal saltation model robustly predicts both the observed scaling and a new undersaturated steady transport state that we confirm by simulations for rarefied atmospheres.

DOI: 10.1103/PhysRevLett.130.058204

Sand is a baffling material. It resembles a gas when shaken, a liquid when poured down a chute, and a solid when resting at a beach. When it is carried along by wind, all three manifestations are crucially involved side by side, making such aeolian transport a most revealing but also quite intricate sand-transport mode [1]. It is responsible for the spontaneous emergence of a multitude of granular surface waves in a variety of inorganic and organic sands, throughout the Solar System [2]. Surprisingly, it also relates them to the drained halos that brighten up around your feet when you step on wet sand. To establish this connection, we start from an empirically discovered scaling of the aeolian sand-transport rate $Q(s, v_s, \tau)$ as a function of the particle-fluid density ratio s ($s \approx 2100$ for quartz in air and $s \approx 2.65$ in water), terminal grain settling velocity v_s, and wind shear stress τ [3]. In natural units, based on the grains' median diameter and mass density, and the buoyancy-reduced gravitational acceleration $\tilde{g} \equiv (1 - 1/s)g$, it reads (Fig. 1)

$$Q = (\tau - \tau_t)[1 + 7.6(\tau - \tau_t)]V, \quad \text{with} \tag{1a}$$

$$V = 1.6 s^{1/3}. \tag{1b}$$

This formulation splits the overall transport rate Q into what is essentially the average velocity V and density $\tau - \tau_t > 0$ of mobilized grains [4]. Intriguingly, the transport threshold $\tau_t(s, v_s)$ completely encapsulates the strength and functional form of fluid-particle interactions [3]. The usually subdominant term $7.6(\tau - \tau_t)$ is a semiempirical attempt to account for cooperative effects induced by intense winds, chiefly sand bed fluidization and midair grain collisions [5–8]. In the opposite limit, $\tau \approx \tau_t$, aeolian transport is idealized in terms of individual grains hopping along a static bed while dislodging additional grains, parametrized through a local "splash function" [9–12], in the standard modeling approach [8,13–34]. However, these conventional saltation models fail to recover Eq. (1b), whose pure s dependence and insensitivity to v_s clashes with physical intuition and naive dimensional analysis [3].

The primary objective of this Letter is to demonstrate a physical mechanism leading to such anomalous scaling. To

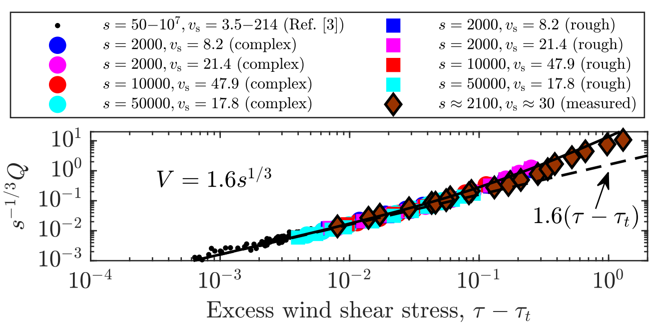

FIG. 1. Data from laboratory measurements [7,23,35] and previous [3] as well as our original sand-transport simulations, based on the discrete element method (DEM) [36,37] (see Supplemental Material [38] for details), obey the transport-rate scaling in Eqs. (1a) and (1b) (solid line). The DEM simulations allow us to toggle between a complex boundary-layer wind velocity profile (dots and circles) and simplified "fully rough" flow conditions (squares) based on Prandtl's turbulent closure [42], cf. Eq. (2c), and to study a wide range of particle-fluid density ratios s, terminal grain settling velocities v_s, and shear stresses τ in excess of the transport threshold τ_t. The dashed line amounts to neglecting midair grain collisions.

this end, we first show that the mentioned failure of conventional saltation models is of general nature and hints at a coupling between the gaslike saltation layer and the rheology of the dense sand bed. The bed cannot be represented by a purely static granular packing, with a static-bed (local) splash function. Our discrete element method (DEM) simulations indeed reveal bed creep well below the yield point. While its direct contribution to Q is negligible, bed creep and its concomitant nonlocal dilatancy cooperatively couple individual grain-bed collisions. Including this effect within a minimal analytical saltation model via a cooperative, dilatancy-enhanced splash function indeed reproduces Eq. (1b) and makes further testable predictions.

Consider a two-dimensional Cartesian coordinate system (x, z), with wind direction x and vertical direction z. For fluid-particle interactions via buoyancy and (for simplicity Stokes) drag, implying a terminal grain settling velocity $v_s = s/(18\nu)$ with the kinematic atmospheric viscosity ν, the equations of motion for the ith grain trajectory ($i = 1, \ldots, N$) read

$$\dot{v}_z^i = -1 - v_z^i/v_s, \tag{2a}$$

$$\dot{v}_x^i = (u_x - v_x^i)/v_s, \tag{2b}$$

$$\kappa^2(z+z_0)^2 u_x'|u_x'| = u_*^2[1-\tau_g(z)/\tau], \quad u_x(0) = 0. \tag{2c}$$

The last equation is Prandtl's turbulent closure [42] for the wind velocity field $u_x(z)$ in the steady state, with the von Kármán constant $\kappa = 0.4$, aerodynamic bed roughness $z_0 = 1/30$, wind shear velocity $u_* \equiv \sqrt{s\tau}$, and grain-borne shear stress profile $\tau_g(z)$. As the xz component of the granular stress tensor (σ_{ij}), the latter accounts for the streamwise momentum transfer between the wind and the grains along all grain trajectories: $\tau_g(z) = \sum_i \phi^i \Delta v_x^i(z)$. Here, ϕ^i is the vertical flux of grains contributed by the ith trajectory and $\Delta v_x^i(z)$ the streamwise velocity gained between its ascending and descending visits of the elevation z. In the absence of grain motion ($\phi^1, \ldots, \phi^N = 0$), Prandtl's closure recovers the well-known (fully rough) law of the wall, $u_x = \kappa^{-1} u_* \ln(1 + z/z_0)$. To close Eqs. (2a)–(2c), they are combined with a splash function, consisting of $2N$ boundary conditions linking the grain trajectories' impact velocities $\boldsymbol{v}_\downarrow^i$ to their lift-off velocities $\boldsymbol{v}_\uparrow^i$, and N boundary conditions interconnecting the vertical flux contributions ϕ^i. Importantly, for conventional, static-bed splash functions, all boundary conditions are fully determined by the impact velocities $\boldsymbol{v}_\downarrow^i$ [9–11]. Hence, for given values of v_s and u_*, the combined system of equations is closed and therefore has a fully determined solution $(\boldsymbol{v}^i, \phi^i/\tau)$. From this solution, all relevant global transport properties can be derived if also s and thus $\tau = u_*^2/s$ are known. However, in blatant conflict with this analysis, V in Eq. (1b) is found to be independent of both v_s and u_*, also in DEM simulations employing Prandtl's turbulent closure (Fig. 1).

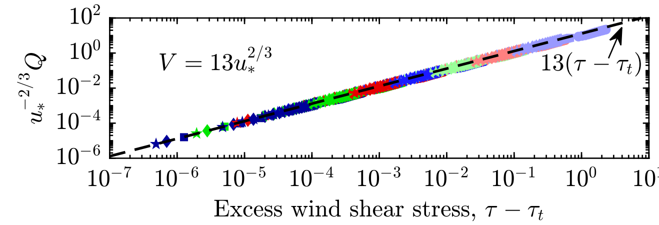

FIG. 2. Sand transport rate scaling predicted by our minimal two-species saltation model without midair collisions [$Q = (\tau - \tau_t)V$] and with a static-bed splash function [9] for terminal grain settling velocities $v_s = \{10^{3/2}, 10^2, 10^{5/2}, 10^3\}$ (circles, squares, diamonds, stars) and particle-fluid density ratios $s = \{4^0, \ldots, 4^6\}v_s^2/10$ (colors). Small (large) s tend to be on the right (left).

Nonetheless, even the simplest nontrivial version of the above general model constitutes a minimal saltation model [38] that can analytically reveal the origin of this discrepancy. It combines the common [30,32] simplification of only considering two representative grain trajectories, namely high-energy saltons that rebound upon impact and their low-energy ejecta, the so-called reptons, with a closure mimicking the mass conservation found in the actual steady state [38,43]. With boundary conditions gleaned from an experimentally measured splash function for a quiescent bed [9], the calculated steady-state solutions $Q(\tau - \tau_t)$ (for saturated transport conditions) admit a data collapse consistent with $V = 13u_*^{2/3}$ (Fig. 2), in line with previous observations based on (single- and multispecies) saltation models utilizing diverse static-bed splash functions [30–34]. The scaling results from the height-dependent feedback of the grain trajectories on the wind. It seems, however, at odds with the widespread belief that the experimentally observed insensitivity of V to the wind shear velocity u_* is a consequence of the splash process [43,44].

To resolve this apparent paradox, notice that, by dividing the right hand side of the relation $V = 13u_*^{2/3}$ by $\tau^{1/3} = (u_*^2/s)^{1/3}$, one gets rid of the spurious u_* dependence of V, and consistency with Eq. (1b) is restored. While this procedure is inconsistent with the notion of a static-bed splash, we now show how it emerges by cooperative splash from a bed that is locally partially mobilized from earlier salton impacts. As revealed by Fig. 3(a), the intermittent bed mobilization by impacting grains gives rise to a net granular creep upon averaging [45]. The penetration of the emerging average grain velocity profile into the bed is characterized by a τ-invariant skin depth λ on the order of the grain diameter and associated with a considerable dilation of the bed, extending to a comparable depth [Fig. 3(b)]. Additionally, our DEM simulations reveal an extended $\mu(I)$-rheological master relation [46,47] below the yield point [Fig. 3(c)].

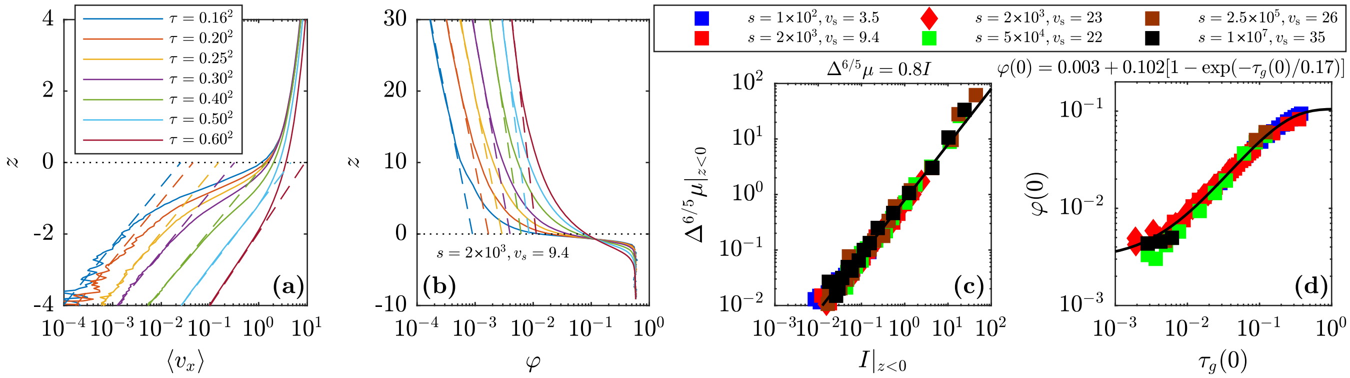

FIG. 3. Quasi-two-dimensional DEM-based sand-transport simulations (as in Ref. [3]) of the creep and dilatancy regime of aeolian transport. (a) Granular creep visualized by the average height-resolved horizontal grain velocity $\langle v_x\rangle(z)$ in the sediment bed ($z<0$, below the elevation at which high-energy grain-bed collisions occur [4,38]). Its increase with height z and imposed wind shear stress τ (solid lines) reveals a characteristic skin depth $\lambda \approx 0.72$ (dashed lines). (b) Because of progressive smoothing, the granular volume fraction profiles $\varphi(z)$ (solid lines) around $z=0$ deviate considerably from the limiting form for saltation on a quiescent bed—roughly a step from $\varphi \approx 0.58$ to the exponential extrapolations of $\varphi(z>0)$ (dashed lines) [23,35]. They exhibit a focal point $\varphi_f = \varphi(z\approx -\lambda) \approx 0.1$. (c) The constitutive relation $\mu(\Delta, I)$ (solid line) for aeolian creep at subyield conditions ($\mu \lesssim 0.3$) is similar to that of other sheared granular flows [46,47]. It interconnects the local friction coefficient $\mu = -\sigma^c_{xz}/\sigma^c_{zz}$, local normalized streamwise velocity fluctuations $\Delta \equiv (-T_{xx}/\sigma^c_{zz})^{1/2}$ with $T_{xx} \equiv \langle v_x^2\rangle - \langle v_x\rangle^2$, and local inertial number $I \equiv \langle dv_x/dz\rangle/\sqrt{-\sigma^c_{zz}}$. Here, σ^c_{xz} (σ^c_{zz}) is the shear (normal) component of the structural granular stress associated with grain-grain contacts in the bed [38]. (d) The value $\varphi(z=0)$ is taken as a proxy for the number of grains available for splash ejection in Eq. (3), and its $\tau_g(0)$ dependence motivates Eq. (4) with $\tau_Y \approx 0.17$.

That it holds over a wide range of transport conditions establishes aeolian creep as a complex but well defined rheological phenomenology. Its robust constitutive law links the slow granular shearing motion driven by grain-bed collisions to the dissipation into (and the heating of) the bed. Its direct contribution to the overall transport rate Q and momentum and energy dissipation is negligible—what matters is its indirect contribution via the dilatancy effect that enhances a subsequent splash and thereby boosts the highly dissipative repton layer [30].

To understand how this comes about, consider again Fig. 3(b). For growing τ, the step function of the granular volume fraction $\varphi(z)$ observed for a quiescent bed is increasingly smoothed, with an invariable focal point at $\varphi_f = \varphi(z\approx -\lambda) \approx 0.1$. This is the dilatancy effect: a close-packed granular bed is jammed and cannot be sheared without dilating it to create free volume for the necessary grain rearrangements. It is the very mechanism that causes the aforementioned drainage and halos around the feet of beach walkers [48]. As naturally expected, dilatancy affects the splash. In fact, recent DEM simulations have indicated an increase of the number N_e of ejected bed-surface grains per salton with increasing impact frequency, while other splash properties such as the ejecta velocities remain nearly unaffected [49]. Since bed grains are effectively trapped (like in a Newton cradle), while hopping grains detach from their force chains, we assume that N_e is directly proportional to the granular volume fraction $\varphi(0)$ at the rebound height $z=0$ (the “mechanically pertinent bed surface,” $\lambda \approx 0.72$ above the focal depth) [4,38]:

$$N_e/N_e^{\rm stat} = \varphi(0)/\varphi^{\rm stat}(0). \tag{3}$$

This simple schematic model couples the gaslike layer of hopping grains above the bed surface to the dense-bed dynamics underneath and represents a crucial upgrade of the conventional static-bed splash parametrization, accounting for the dilatancy-mediated cooperativity. Remarkably, the observed splash geometry—in particular its characteristic surface radius $R = \mathcal{O}(10)$ [11,49] and associated mobilized bed volume $N_e^{\rm stat}/\varphi^{\rm stat} \simeq 6R^2\lambda = \mathcal{O}(600\lambda)$—is, together with $\varphi(0) \to \varphi^{\rm stat}(0) \approx 3\times10^{-3}$ in the static-bed limit [Fig. 3(d)], indeed consistent with the observation $N_e \to N_e^{\rm stat} = \mathcal{O}(1)$ [9–12].

Granular creep has been characterized as a sequence of stick-slip events, whereby slipping occurs when local fluctuations of the friction coefficient μ exceed the yield point [45]. In our context of aeolian creep, characterized by its impact-induced local bed mobilizations with constant skin depth $\lambda = \mathcal{O}(1)$, μ reduces to the surface grain-borne shear stress $\tau_g(0)$ in our natural units [50]. Indeed, our DEM simulations show that Eq. (3) is solely controlled by $\tau_g(0)$ via [Fig. 3(d)]:

$$\varphi(0) = \varphi^{\rm stat}(0) + \varphi_f[1-\exp(-\tau_g(0)/\tau_Y)]. \tag{4}$$

The linear growth, $\varphi(0) = \varphi^{\rm stat}(0) + \varphi_f\tau_g(0)/\tau_Y$, for small $\tau_g(0)$ saturates near φ_f (at $N_e = 35N_e^{\rm stat}$) for large $\tau_g(0)$ [cf. Fig. 3(b)]. This suggests that the focal-point volume fraction φ_f can be interpreted as the maximum φ of fully

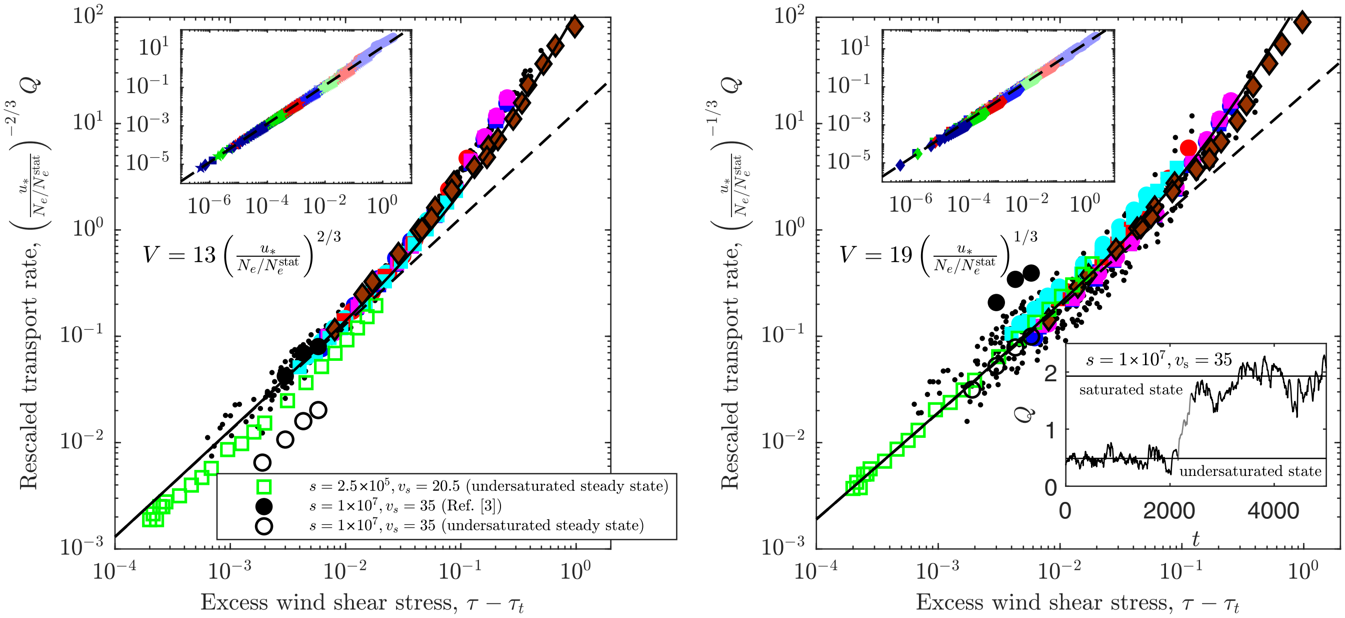

FIG. 4. Laboratory measurements, DEM-based sand-transport simulations (cf. Fig. 1), and predictions by our minimal saltation model with cooperative splash according to Eqs. (3) and (4) (inset) collapse on a master curve defined by (a) Eqs. (1a) and (5) (approximately $V \propto s^{1/3}$), corresponding to saturated transport conditions, or (b) an undersaturated steady state [Eqs. (1a) and (6), approximately $V \propto s^{1/6}$, upper inset]. Depending on the initial condition, this state can also be reached and sustained in DEM simulations, based on the code of Ref. [3] (open black circles) or Ref. [37] (open green squares) for $s \gtrsim 10^5$, regardless of the driving flow velocity profile (cf. Fig. 1). Lower inset: exemplary transition between the steady states, as occasionally spotted in the simulations. Solid (dashed) lines correspond to Eqs. (1a) and (1b) with (without) the term representing midair collisions, which are neglected in our minimal saltation model. Filled symbols as in Figs. 1 and 2.

mobile grains and therefore parametrizes a "critical bed dilation," below which bed force chains effectively disintegrate. The characteristic value $\tau_Y \approx 0.17$, which determines both the linear increase and the saturation behavior in Eq. (4), can be linked to the yield friction $\mu_Y = \tau_Y/\varphi_b$ (for spheres, $\mu_Y \approx 0.3$ [45]) associated with an elementary yield event of a single bed grain at the static-bed volume fraction $\varphi_b \approx 0.58$. In the same spirit, $\tau_Y/\varphi_f \approx 1.7$ plays the role of a critical granular shear temperature required for grains to escape their traps and leapfrog over neighboring grains [23].

As shown in Fig. 4(a), data from our upgraded minimal saltation model, with cooperative splash according to Eqs. (3), (4), and $\tau_g(0) = \tau - \tau_t$ [4], collapse on

$$V = 13\left(\frac{u_*}{N_e/N_e^{\rm stat}}\right)^{2/3}, \tag{5}$$

the master curve of the simulation and laboratory data. As expected, the transport threshold τ_t is not affected by this upgrade. The linear approximation of Eq. (4) with $1 + (\tau - \tau_t)/\tau_e \approx 2[(\tau - \tau_t)/\tau_e]^{1/2}$ [arithmetic mean ≈ geometric mean, where $\tau_e \equiv \tau_Y \varphi^{\rm stat}(0)/\varphi_f \approx 5 \times 10^{-3}$] yields $V \approx 1.4(1 - \tau_t/\tau)^{-1/3} s^{1/3}$, deviating less than 13% from Eq. (1b) when $\tau/\tau_t \gtrsim 2$. The anomalous scaling (compared to $V = 13u_*^{2/3}$ for static-bed splash) has thus been traced back to the strongly skewed mass balance between reptons and saltons, originating from the creep-associated bed dilatancy. While their individual streamwise velocities exhibit the same increase with u_* as in the static-bed case, the fraction of reptons increases by an order of magnitude with growing $\tau - \tau_t$, resulting in an almost τ-invariant V.

Intriguingly, we moreover find that the steady-state condition in our minimal saltation model innately allows for an additional, undersaturated steady transport state [upper inset of Fig. 4(b)], which scales as

$$V = 19\left(\frac{u_*}{N_e/N_e^{\rm stat}}\right)^{1/3}. \tag{6}$$

Our DEM simulations indeed confirm its existence over a range of environmental conditions [Fig. 4(b)]. For $s \lesssim 10^5$, all simulations seem to approach the saturated steady state described by Eq. (5), while some simulations for $s \gtrsim 10^5$ can reach both steady states, Eq. (5) or (6), for the explored initial conditions. Large random fluctuations can induce transitions between the steady states [lower inset of Fig. 4(b)]. In view of the complexity of aeolian transport, the simultaneous quantitative agreement of both predicted steady states with grain-scale simulations provides strong support for our minimal two-species saltation model with cooperative splash.

In conclusion, we have shown that cooperative granular dynamics within the sand bed substantially affects aeolian sand-transport characteristics and can account for the anomalous scaling of the sand-transport rate $Q(s, v_s, \tau)$ [Eqs. (1a) and (1b)]. The upshot is that grain-bed collisions cannot be portrayed as a sequence of isolated impacts on a purely static bed, but cooperate indirectly via the nonlocal and somewhat counterintuitive effect of creep-associated bed dilatancy. The main physical consequence is an increase of the relative population of (low-energy) reptating grains, which act as a momentum sink to the atmospheric boundary-layer flow. Our analytical two-species minimal saltation model, incorporating only a single representative salton and repton trajectory, respectively, identifies this cooperative, dilatancy-mediated negative feedback as the root cause behind the somewhat perplexing insensitivity of the average sand-transport velocity V against substantial variations of the wind shear velocity u_*—thus challenging previous explanation attempts. Interestingly, it innately predicts an additional, undersaturated steady transport state, confirmed by our DEM simulations for conditions with extreme particle-fluid density ratio ($s \gtrsim 10^5$), as typical for the thin atmospheres of Mars and Pluto. This calls for future studies of the competition between the two steady states in natural environments. It is also strongly indicative of the suitability of our analytical two-species saltation model for addressing the physical mechanism underlying other characteristic traits of aeolian transport.

This research was supported by a grant from the GIF, the German-Israeli Foundation for Scientific Research and Development (No. 155-301.10/2018). Furthermore, we acknowledge support from the National Natural Science Foundation of China (No. 12272344) and thank the German Research Foundation for funding through the Heisenberg Programme and the Grant No. 348617785. We particularly acknowledge the Regional Computing Center (RRZK) of the University of Cologne and the Centre for Information and Media Service (ZIM) of the University of Duisburg-Essen for computing time provided on the HPC systems CHEOPS and MagnitUDE, respectively.

[*]0012136@zju.edu.cn
[†]klaus.kroy@uni-leipzig.de

[1] R. A. Bagnold, *The Physics of Blown Sand and Desert Dunes* (Methuen, New York, 1941).

[2] A. G. Hayes, Dunes across the solar system, Science **360**, 960 (2018).

[3] T. Pähtz and O. Durán, Scaling laws for planetary sediment transport from DEM-RANS numerical simulations, arXiv:2203.00562.

[4] T. Pähtz and O. Durán, Universal friction law at granular solid-gas transition explains scaling of sediment transport load with excess fluid shear stress, Phys. Rev. Fluids **3**, 104302 (2018).

[5] J. M. Pasini and J. T. Jenkins, Aeolian transport with collisional suspension, Proc. R. Soc. A **363**, 1625 (2005).

[6] M. V. Carneiro, N. A. M. Araújo, T. Pähtz, and H. J. Herrmann, Midair Collisions Enhance Saltation, Phys. Rev. Lett. **111**, 058001 (2013).

[7] J. L. Ralaiarisoa, J. B. Besnard, B. Furieri, P. Dupont, A. Ould El Moctar, F. Naaim-Bouvet, and A. Valance, Transition from Saltation to Collisional Regime in Windblown Sand, Phys. Rev. Lett. **124**, 198501 (2020).

[8] T. Pähtz and O. Durán, Unification of Aeolian and Fluvial Sediment Transport Rate from Granular Physics, Phys. Rev. Lett. **124**, 168001 (2020).

[9] D. Beladjine, M. Ammi, L. Oger, and A. Valance, Collision process between an incident bead and a three-dimensional granular packing, Phys. Rev. E **75**, 061305 (2007).

[10] M. Lämmel, K. Dzikowski, K. Kroy, L. Oger, and A. Valance, Grain-scale modeling and splash parametrization for aeolian sand transport, Phys. Rev. E **95**, 022902 (2017).

[11] T. Tanabe, T. Shimada, N. Ito, and H. Nishimori, Splash detail due to a single grain incident on a granular bed, Phys. Rev. E **95**, 022906 (2017).

[12] F. Comola and M. Lehning, Energy- and momentum-conserving model of splash entrainment in sand and snow saltation, Geophys. Res. Lett. **44**, 1601 (2017).

[13] P. R. Owen, Saltation of uniform grains in air, J. Fluid Mech. **20**, 225 (1964).

[14] R. J. Kind, A critical examination of the requirements for model simulation of wind-induced erosion/deposition phenomena such as snow drifting, Atmos. Environ. **10**, 219 (1976).

[15] G. Sauermann, K. Kroy, and H. J. Herrmann, A continuum saltation model for sand dunes, Phys. Rev. E **64**, 031305 (2001).

[16] J. J. J. Doorschot and M. Lehning, Equilibrium saltation: Mass fluxes, aerodynamic entrainment, and dependence on grain properties, Boundary-Layer Meteorol. **104**, 111 (2002).

[17] M. Sørensen, On the rate of aeolian sand transport, Geomorphology **59**, 53 (2004).

[18] M. P. Almeida, J. S. Andrade, and H. J. Herrmann, Aeolian Transport Layer, Phys. Rev. Lett. **96**, 018001 (2006).

[19] O. Durán and H. J. Herrmann, Modelling of saturated sand flux, J. Stat. Mech. (2006) P07011.

[20] M. P. Almeida, E. J. R. Parteli, J. S. Andrade, and H. J. Herrmann, Giant saltation on Mars, Proc. Natl. Acad. Sci. U.S.A. **105**, 6222 (2008).

[21] T. Pähtz, J. F. Kok, and H. J. Herrmann, The apparent roughness of a sand surface blown by wind from an analytical model of saltation, New J. Phys. **14**, 043035 (2012).

[22] J. E. Ungar and P. K. Haff, Steady state saltation in air, Sedimentology **34**, 289 (1987).

[23] M. Creyssels, P. Dupont, A. Ould El Moctar, A. Valance, I. Cantat, J. T. Jenkins, J. M. Pasini, and K. R. Rasmussen, Saltating particles in a turbulent boundary layer: Experiment and theory, J. Fluid Mech. **625**, 47 (2009).

[24] J. T. Jenkins and A. Valance, Periodic trajectories in aeolian sand transport, Phys. Fluids **26**, 073301 (2014).

[25] D. Berzi, J. T. Jenkins, and A. Valance, Periodic saltation over hydrodynamically rough beds: Aeolian to aquatic, J. Fluid Mech. **786**, 190 (2016).

[26] J. T. Jenkins and A. Valance, Two-phase continuum theory for windblown sand, Phys. Rev. Fluids **3**, 034305 (2018).

[27] B. Andreotti, P. Claudin, J. J. Iversen, J. P. Merrison, and K. R. Rasmussen, A lower than expected saltation threshold at Martian pressure and below, Proc. Natl. Acad. Sci. U.S.A. **118**, e2012386118 (2021).

[28] T. Pähtz, Y. Liu, Y. Xia, P. Hu, Z. He, and K. Tholen, Unified model of sediment transport threshold and rate across weak and intense subaqueous bedload, windblown sand, and windblown snow, J. Geophys. Res. **126**, e2020JF005859 (2021).

[29] X. Huo, H. Dun, N. Huang, and J. Zhang, 3D direct numerical simulation on the emergence and development of aeolian sand ripples, Front. Phys. **9**, 662389 (2021).

[30] B. Andreotti, A two-species model of aeolian sand transport, J. Fluid Mech. **510**, 47 (2004).

[31] J. F. Kok and N. O. Renno, A comprehensive numerical model of steady state saltation (COMSALT), J. Geophys. Res. **114**, D17204 (2009).

[32] M. Lämmel, D. Rings, and K. Kroy, A two-species continuum model for aeolian sand transport, New J. Phys. **14**, 093037 (2012).

[33] M. Lämmel and K. Kroy, Analytical mesoscale modeling of aeolian sand transport, Phys. Rev. E **96**, 052906 (2017).

[34] F. Comola, J. F. Kok, J. M. Lora, K. Cohanim, X. Yu, C. He, P. McGuiggan, S. M. Hörst, and F. Turney, Titan's prevailing circulation might drive highly intermittent, yet significant sediment transport, Geophys. Res. Lett. **49**, e2022GL097913 (2022).

[35] T. D. Ho, A. Valance, P. Dupont, and A. Ould El Moctar, Scaling Laws in Aeolian Sand Transport, Phys. Rev. Lett. **106**, 094501 (2011).

[36] O. Durán, B. Andreotti, and P. Claudin, Numerical simulation of turbulent sediment transport, from bed load to saltation, Phys. Fluids **24**, 103306 (2012).

[37] S. Kamath, Y. Shao, and E. Parteli, Scaling laws in aeolian sand transport under low sand availability, Geophys. Res. Lett. **49**, e2022GL097767 (2022).

[38] See Supplemental Material at http://link.aps.org/supplemental/10.1103/PhysRevLett.130.058204, which includes Refs. [39–41], for numerical model details, computation of physical quantities from the simulation data, and derivation of the minimal trajectory model.

[39] T. Pähtz, O. Durán, T.-D. Ho, A. Valance, and J. F. Kok, The fluctuation energy balance in non-suspended fluid-mediated particle transport, Phys. Fluids **27**, 013303 (2015).

[40] T. Pähtz and O. Durán, Fluid forces or impacts: What governs the entrainment of soil particles in sediment transport mediated by a Newtonian fluid?, Phys. Rev. Fluids **2**, 074303 (2017).

[41] T. Pähtz and O. Durán, The cessation threshold of non-suspended sediment transport across aeolian and fluvial environments, J. Geophys. Res. **123**, 1638 (2018).

[42] L. Prandtl, Über die ausgebildete Turbulenz, Z. Angew. Math. Mech. **5**, 136 (1925).

[43] O. Durán, P. Claudin, and B. Andreotti, On aeolian transport: Grain-scale interactions, dynamical mechanisms and scaling laws, Aeolian Res. **3**, 243 (2011).

[44] J. F. Kok, E. J. R. Parteli, T. I. Michaels, and D. B. Karam, The physics of wind-blown sand and dust, Rep. Prog. Phys. **75**, 106901 (2012).

[45] T. Pähtz, A. H. Clark, M. Valyrakis, and O. Durán, The physics of sediment transport initiation, cessation, and entrainment across aeolian and fluvial environments, Rev. Geophys. **58**, e2019RG000679 (2020).

[46] J. Gaume, G. Chambon, and M. Naaim, Microscopic Origin of Nonlocal Rheology in Dense Granular Materials, Phys. Rev. Lett. **125**, 188001 (2020).

[47] S. Kim and K. Kamrin, Power-Law Scaling in Granular Rheology Across Flow Geometries, Phys. Rev. Lett. **125**, 088002 (2020).

[48] See video visualizing the drainage in response to shear-induced dilation of sand: https://www.youtube.com/watch?v=kzw80pyUI8g.

[49] S. Jia and Z. Wang, A new ejection model for aeolian splash, Catena **213**, 106191 (2022).

[50] A. H. Clark, J. D. Thompson, M. D. Shattuck, N. T. Ouellette, and C. S. O'Hern, Critical scaling near the yielding transition in granular media, Phys. Rev. E **97**, 062901 (2018).